Lab on a Chip

Accepted Manuscript

ROYAL SOCIETY OF CHEMISTRY

www.rsc.org/loc

Journal Name

RSCPublishing

ARTICLE

Convection-driven long-range linear gradient generator with dynamic controls

Cite this: DOI: 10.1039/x0xx00000x

Hao Wang[a,c], Chia-Hung Chen[b,c], Zhuolin Xiang [a,c], Ming Wang[b,c] and Chengkuo Lee[a,c*]

Received 00th January 2012,
Accepted 00th January 2012

DOI: 10.1039/x0xx00000x

www.rsc.org/

We developed a novel gradient generator to achieve long range and linear chemical gradient with dynamic control function. The length of the gradient can be at centimetre scale. The gradient profile can be tuned by changing the flow rates. The device can work in both high flow rate regime with large shear stress and low flow rate with minimum shear stress. The function of drug screening is demonstrated by the viability test of PC-9 cancer cells.

Introduction

Nowadays, engineering various gradients has attracted extensive attention for biomedical applications because gradients play essential roles in many biological activities and regulate a number of cellular functions *in vivo*. Chemical gradients have been shown to affect various cell behaviours, such as migration, proliferation, and differentiation during development[1,2]. Microfluidic devices offer the possibility of generating complex and well defined gradient profiles.

One of the most popular methods to generate the chemical gradient is to leverage the Christmas Tree design[3-20]. Two or more fluids are mixed with different ratio by a channel network and form the gradient in a main channel by laminar flow. Because of the laminar regime that is inherent to fluid flow in micro-channels, the geometry of the micro-device and the flow rates can be tuned to subject the cultured cells to well-defined, diffusion-independent concentration profiles. However, the use of existing microfluidic gradient generators encounters hydrodynamic shear stresses that arise from the small characteristic dimensions of microfluidic channels. For most cultured cells, the maintenance of low levels of hydrodynamic shear is vital for the preservation of their wellbeing. To ensure a good laminar flow and gradient profile in the main channel, the fluid flows out from each small channel should be of symmetric flow rate pattern and different mix ratios of two kinds of fluids[4-17]. The symmetric flow rate pattern could be realized by the symmetric channel network. But this symmetric channel network will induce a non-linear gradient profile. It is very challenging to optimize the channel network which could realize both laminar flow and linear gradient profile. Moreover, since the gradient generated by the laminar flow is not affect by the flow rate, the Christmas tree designs also lack the function of dynamic control of the gradient profile. The initial fluid concentration from the inlet has to be changed if different gradient profile needs to be studied. Since the laminar flow can only maintained in low Reynolds number, the length of the gradient is also limited.

Another major approach is to leverage the diffusion to generate chemical gradient[21-34]. The gradient generated by diffusion is vulnerable to convection flow. Thus the main issue for chemical gradient generator based on diffusion is the isolation of convection flow during the gradient generation procedure. For membrane-based diffusion chips[30-32,34], convection flows are physically isolated by the thin membranes and only chemical molecules are allowed to diffuse through the membrane. For channel-based diffusion chips[28,33], convection flows are minimized by micro-channels whose dimension are much smaller than main channels to maintain chemical gradients. Due to the isolation of convection flow, the gradients are mainly maintain at low or even static flow rate with minimal level of shear stresses which is ideal for cell culture. On the other hand, the duration required to stabilize the gradient is relatively long because of the low flow rate. Once the gradient is formed, it is not easy to have a dynamic control of the gradient profile. Moreover, the gradient profile is mainly determined by the nature of diffusion, the linearity is not guaranteed. To shorten the duration for stabilizing the gradient and enable an easier process for optimization and characterization, the length or area of the gradient are normally limited to hundreds of micrometer scale.

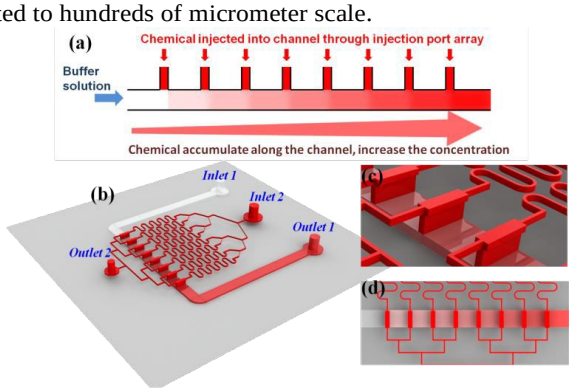

Scheme.1 The working principle and structure of the chemical gradient generator.

Method

Here we present a novel gradient generation method based on convection-driven flow. This approach has many advantages over the methodologies developed so far since it can simultaneously satisfy the following:(1)The length of the gradient can be at centimetre scale and the time to stabilize the gradient is short; (2) A linear gradient profile which cannot be

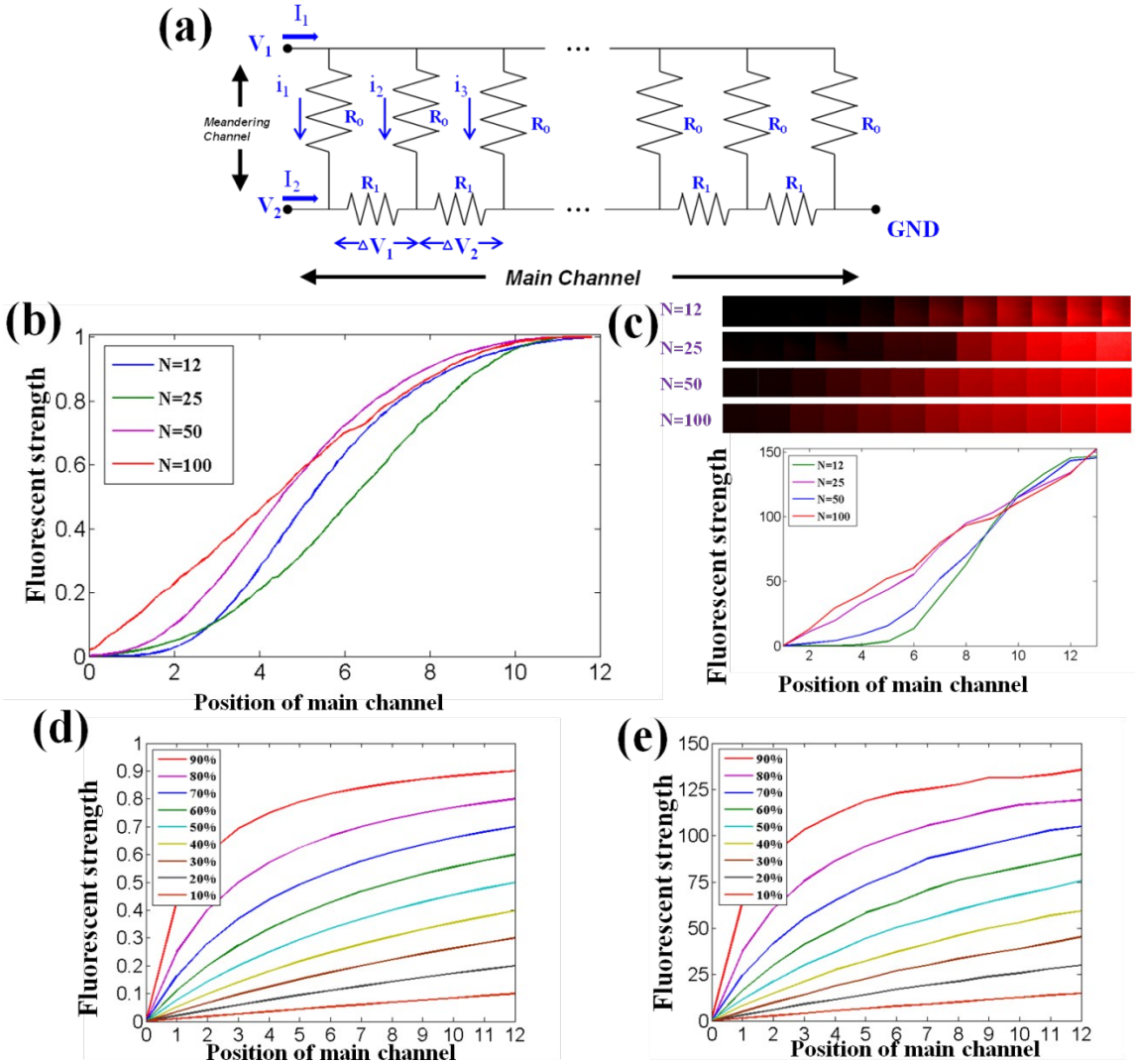

Fig. 1 (a) Discrete fluidic circuit model of the gradient generator; (b) Simulation results of gradient profiles by changing the length of meandering channels; (c) Experiment results of fluorescent images and gradient profiles by changing the length of meandering channels; (d) Ideal curve of the gradient profiles when changing the final concentration at end point; (e) Experiment results of gradient profiles when changing the final concentration at end point when N=50.

realized by Christmas tree designs and diffusion based designs. Thus concentration gradient profiles can be relatively easily predicted (3) The linear gradient profile is tuneable by changing the flow rates just by changing the flow rate which is not feasible by Christmas tree design and diffusion based design. (4) The device can work in both high flow rate regime with large shear stress and low flow rate regime with minimum shear stress.

Analysis and Characterization

The principle of the gradient generator is shown in Scheme. 1(a).An array of injection ports is connected to the main channel. The chemical solution is added into the flow of buffer solution in main channel through injection ports. Due to the convection flow in main channel, each segment of the main channel will have the accumulation of the chemical injected from the injection ports before this segment. Thus along the main channel, the concentration of the gradient will increase and a chemical gradient is formed. The device to realize this method is shown in Scheme 1(b). The device has a 3D structure with three layers. For the bottom layer, the channel of U-shape is the main channel to generate the chemical gradient. The buffer solution is injected from the inlet 1 of main channel and extracted from outlet 1. Along the main channel, there is an array of vertical injection ports in the middle layer. For the top layer, a channel network connects all the vertical injection ports. The chemical to generate the gradient is introduced from the inlet 2 and injected into the main channel through the injection ports. This channel network looks similar with the channel network used in the Christmas tree design. But the structure and function of these two channel networks are different. In Christmas tree design, two or more inlets are connected to the channel network and the main function of the channel network is to mix the fluids from inlets with different ratio. In our design, the meandering channel network is connected to one inlet and designed to minimize the difference of the injection rate of each vertical injection port, achieving an linear gradient profile. The outlet 2 is designed to avoid any bubbles remain in the channel during the solution filling process at the

beginning of the experiment. The detailed fabrication process and device characterization can be found in Fig. S1.

In this design, the length of the meandering channels is optimized to realize a linear gradient profile. However, the linear

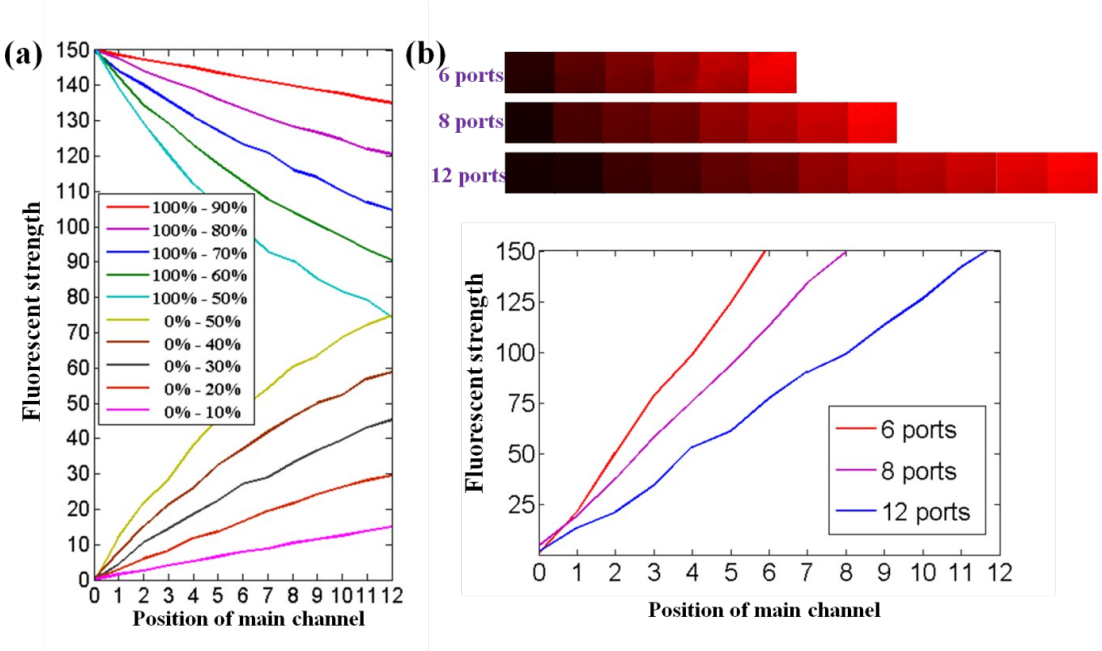

Fig.2 (a) Experiment results of gradient profile using accumulation method and dilution method. Gradient profiles starting from 100% were done by dilution method. Gradient profiles starting from 0% were by accumulation method; (b) Experiment results of gradient profiles from devices of different number of ports.

gradient profile can only cover the range from 0% to 50%. Thus a complementary method was developed to generate a gradients which can cover the range from 100% to 50%. Then a linear gradient of whole range from 0% to 100% can be generated by this gradient generator. At last, the viability tests of PC-9 cancer cells were conducted to demonstrate the capability of drug screening by using this device.

To realize a linear gradient profile, the injection rate of each injection port at different position of the main channel is expected to be identical. The flow rates of injection ports are affected by the pressure applied at the connection part of injection port and main channel which varies with the position along the main channel. To minimize the difference of the flow rates of injection ports, a discrete fluidic circuit model was built as shown in Fig. 1(a) to analyze injection flow rates through the injection port array. The pressure applied on inlet 1 and inlet 2 is $\boldsymbol{V_1}$ and $\boldsymbol{V_2}$ respectively. To simplify the design and optimization, the length of each meandering channel is identical. Thus the flow resistance of each meandering channel from inlet 2 to its injection port is the same, $\boldsymbol{R_0}$. The spacing of the injection port array is the same. So the flow resistance of the channel between two adjacent injection ports is the same, $\boldsymbol{R_1}$. The flow rate through each meandering channel is $\boldsymbol{i_1}$ to $\boldsymbol{i_n}$. Due to the flow through the U-shape channel, there is a pressure drop along the channel. The pressure difference between two adjacent injection ports is from $\Delta\boldsymbol{V_1}$ to $\Delta\boldsymbol{V_n}$.

For injection port $\boldsymbol{n}$ and $\boldsymbol{n+1}$, the flow rate is $\boldsymbol{i_n}$ and $\boldsymbol{i_{n+1}}$. The flow rate difference is

$$\Delta \boldsymbol{i_n} = \boldsymbol{i_{n+1}} - \boldsymbol{i_n} = \frac{\Delta \boldsymbol{V_n}}{\boldsymbol{R_0}}$$

To ensure the linear gradient profile, the chemical concentration should have a linear increase along the U-shape channel. Thus the flow rate through each injection port should be the same. But due to the $\Delta\boldsymbol{V}$ induced by the flow resistance of the channel between two adjacent injection ports, the $\Delta\boldsymbol{i}$ cannot be zero. However, when $\boldsymbol{R_0}$ is close to infinite, the $\Delta\boldsymbol{i}$ can be close to zero. Fig. 1(b) and 1(c) shows representative chemical gradient profile results of mathematical modelling by COMSOL and experiments by using Rhodamine as the fluorescent dye. The number of injection ports is 12 and length of meandering channel ranges from 12 times(N=12) to 100 times(N=100) of the spacing between two adjacent injection ports. The ratio of mass flow rates from inlet 1 and inlet 2 is 1:9 in mathematical modelling. So the final concentration is 10% at the end of main channel. The flow rates to inlet 1 and inlet 2 were 100nl/min and 11.1nl/min respectively in experiments. For the curve N=12, injection ports close to inlet 1 have back flow from the main channel. Thus the concentration is close to zero for the first two ports in the curve. This is because the $\boldsymbol{V_2}$ required to drive the flow rate which is the 1/9 of the flow rate injected from inlet 1 is much lower than $\boldsymbol{V_1}$ when $\boldsymbol{R_0}$ is very small. The flow rate $\boldsymbol{i}$ is negative for the injection ports close to inlet 1. As can be seen from the fluorescent image, the first part is dark. But the sum of the flow rates of all the injection ports is constant. For the after half curve, the injection flow rates of injection ports have a dramatic growth to balance the back flow. When increase the length of meandering channels, $\boldsymbol{R_0}$ becomes larger thus the $\boldsymbol{V_2}$ required to drive the flow also increases. The back flow disappears and the flow rate of each injection port tends to be identical. The profile of the gradient becomes linear when N is larger than 50 as can be seen in Fig. 1(b) and (c).

In general, when N is larger than 50, the difference of the flow rate of the injection port array could be neglected. The output of the injection ports could be considered identical. In this ideal condition, for a device with $\boldsymbol{N}$ injection ports, the chemical concentration of segment $\boldsymbol{n}$ of the main channel is

$$\boldsymbol{C_n} = \frac{\frac{\boldsymbol{n}}{\boldsymbol{N}}\boldsymbol{I_2}}{\boldsymbol{I_1}+\frac{\boldsymbol{n}}{\boldsymbol{N}}\boldsymbol{I_2}} \quad (1)$$

When I_2 is much smaller than I_1, the portion $\frac{n}{N}I_2$ in denominator can be neglected, which is the situation in Fig. 1(b) and (c)($I_2=\frac{1}{9}I_1$,). The profile of the gradient should be completely linear. But the linearity will deteriorate when I_2 increases. Fig. 1(d) shows the ideal curve of equation 1 when the final concentration at the end of channel ranges from 10% to 90% by increasing the I_2. As can be seen in the Fig. 1(d), when the final concentration is not higher than 50%, the linearity is acceptable. The linearity increases with the decrease of final concentration. Once the concentration is larger than 50%, meaning the I_2 is higher than I_1, the portion $\frac{n}{N}I_2$ in denominator takes a greater effect than I_1. Thus the curve is not linear anymore. Fig 1(e) shows the corresponding experiment results with the flow rate of inlet 1 as 100nl/min and N=50. For the results whose final concentration is not higher than 50%, the curve is linear. Once the concentration is higher is 50%, the curve has an obvious upper bending, making the curve not linear. Therefore, by using this method to achieve a linear concentration profile, the final concentration cannot exceed 50%. But within the range from 0% to 50%, the linear gradient profile can have dynamic change just by changing the flow rate ratio from inlet 1 and inlet 2. Due to the linearity of the gradient, when the final concentration is known, which is determined by the flow rate ratio from inlet 1 and inlet 2, the concentration of each segment of the main channel can be predicted.

In general, the function of the channel network in our design is quite different from the channel network used in Christmas tree design. The main purpose of the channel network is to ensure a linear profile rather than realize a solution mixture and laminar flow in Christmas tree design.

Cell viability test

To realize a chemical gradient with range from 0% to 100%, a complementary method was developed. In the previous approach, the maximum linear range for the chemical gradient is 0% to 50%. The chemical solution is injected into the main channel through the injections ports and accumulated along the main channel. It is an accumulation approach. In this complementary method, we give the chemical solution to inlet 1 and buffer solution to inlet 2. Then the linear range of the chemical gradient is from 100% to 50% which is the exact the buffer solution gradient range in the previous method. The chemical solution in main channel is diluted by the buffer solution from injection ports. It is a dilution approach. Fig. 2(a) show the experiment results of accumulation approach and dilution approach respectively. The flow rates of inlet 1 keep 100nl/min, which is low flow rate regime with low shear stress, for all the experiments. All the curves are linear as expected. We also conducted the experiments with the flow rates of inlet 1 as 500nl/min, which is high flow rate regime with high shear stress. The results can be found in Fig. S2 of ESI. All the curves are linear when the flow rates of inlet 1 and inlet 2 keep the same ratio as in Fig. 2(a). The absolute values of flow rates do not introduce obvious effect on the gradient profile when the ratio of flow rates keep the same.

The concentration of different segments are of discrete values in this method. Therefore, the resolution of the gradient is determined by the number of injection ports. More injection ports can give a higher gradient resolution. Fig. 2(b) shows the experiment results of 6, 8 and 12 ports with the same spacing between ports. The final concentrations at end pints are 10%. The N= 50 for all the devices and flow rates for inlet 1 are all 100nl/min. The gradient profiles are all linear. The scale of the injection port array could be further extended to achieve a higher gradient resolution. However,

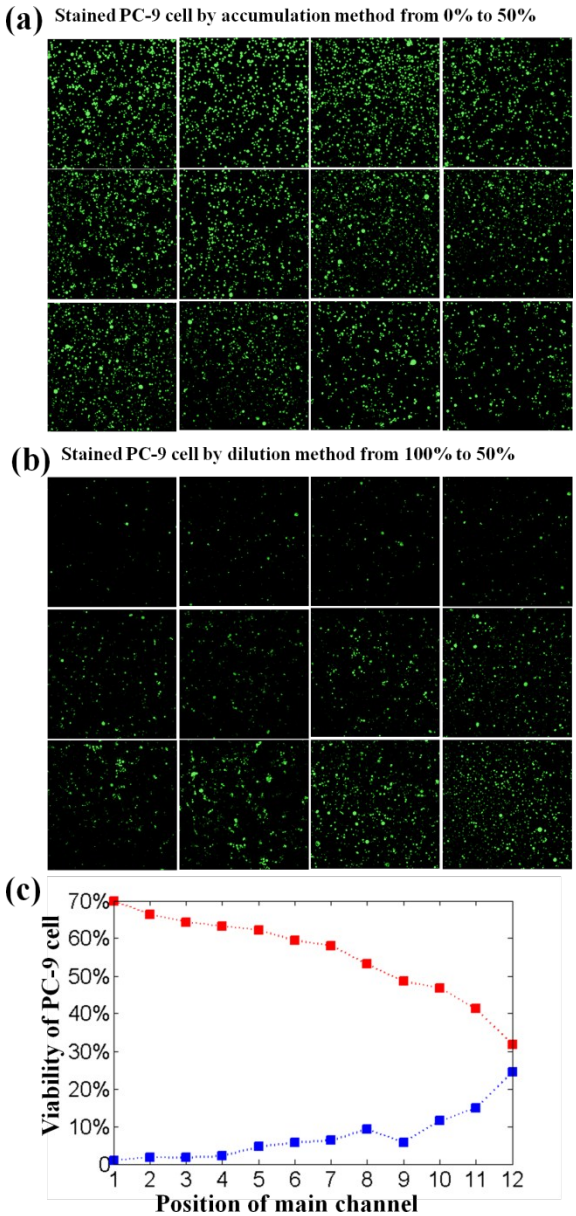

Fig. 4 Experiment of PC-9 cell viability test. (a) Calcein-AM stained PC-9 cancer cells from concentration of 0% to 50% by accumulation method; (b) Calcein-AM stained PC-9 cancer cells from concentration of 100% to 50% by dilution method; (c) Viability of PC-9 cancer cells along the main channel in both accumulation method and dilution method.

the area to distribute the meandering channel will also be enlarged. Hence the devices with more injection ports are not discussed here. Currently the spacing between two adjacent injection ports is 2000μm. Thus for the device with 12 injection ports, the length of the gradient is 2.4 centimetre. The length of the gradient could be further increase by increasing the number of injection ports. This centimetre scale linear gradient profile cannot be realized by either Christmas tree design or diffusion based designs.

To investigate the function of drug screening by using this device, the effect of doxycycline on the viability of PC-9 lung cancer cells was tested. A gradient of doxycycline solution was generated and maintained along the U-shape main channel. The PC-9 cancer cells are immobilized onto the bottom substrate of the main channel. The

detailed process for cell culture and immobilization in U- shape main channel can be found in ESI. The doxycycline solution used in experiment was of 0.8mg/ml concentration. To realize a test range from 0% to 100%, the experiment was divided into two parts. For the first part, the accumulation method was used to generate gradient from 0% to 50%. Doxycycline solution was injected from inlet 2 and culture media was injected from inlet 1. For the second part, the dilution method was used to generate gradient from 100% to 50%. Doxycycline solution was injected from inlet 1 and culture media was injected from inlet 2. All the flow rates from inlet 1 were 100nl/min. The duration of the viability experiment was 2 hours. Calcein-AM staining identified alive cells along the main channel as shown in Fig 3(a) and 3(b). The result of the accumulation method shows a higher cell viability than the result of the dilution method. The viability of cells decreases along the main channel in accumulation method from 70% to around 32% as shown in Fig. 3(c).

In dilution method, the viability of cells increases along the main channel from 2% to around 25%. The final concentrations at the end points of two methods were all 50%. But two curves do not merge together at the end points because of the fluctuation of experiments. As a comparison, the results for the gradient generated by accumulation method from 0% to 90% can be found in Fig. S3 in ESI. Due to the non-linear gradient profile, the result cannot well characterize the viability of cells at all the concentrations.

Conclusions

In summary, we designed and optimized a chemical gradient generator. The chemical gradient range could be tuned by changing the flow rates from the inlets. It could work in both low flow rate regime and high flow rate regime. The resolution of gradient can be improved by adding more injections ports. To achieve a linear gradient profile covering all the range from 0% to 100%, two methods were developed. For accumulation method, the maximum rang was from 0% to 50%. For dilution method, maximum range was from 100% to 50%. Because of the high linearity, the concentrations of different segment can be predicted directly by knowing the position of the segment in the whole channel. This high linearity of the gradient profile cannot be achieved by other gradient generators. Since the convection flow is leveraged to generate the chemical gradient, the length of the gradient could be extended to centimetre scale. The ability for drug screening was demonstrated by the cell viability experiments. In addition, the linear profile, the tunable gradient range and the ability to work with both low and high shear stress make this device rather attractive for a variety of cell-based studies.

Notes and references

[a] H. Wang, Z. Xiang and C. Lee are with the Department of Electrical and Computer Engineering and Singapore Institute for Neurotechnology (SINAPSE), National University of Singapore, Singapore 117576. (e-mail: elelc@nus.edu.sg).

[b] C. Chen and M. Wang are with the Department of Biomedical Engineering and Singapore Institute for Neurotechnology (SINAPSE), National University of Singapore, Singapore,117575.

†Electronic Supplementary Information (ESI) available: [1. Fabrication process; 2. Gradient profile of both accumulation method and dilution method with the flow rate 500nl/min of inlet 1; 3. Detailed process for cell culture and immobilization in U- shape main channel; 4. Viability test of PC-9 cancer cells of the gradient from 0% to 90% generated by accumulation method]. See DOI: 10.1039/c000000x/

1 J. E. Phillips, K. L. Burns, J. M. Le Doux, R. E. Guldberg and A. J. García, *Proc. Natl. Acad. Sci. U. S. A.*, 2008, **105**, 12170–12175.
2 F. Wang, *Cold Spring Harbor Perspect. Biol.*, 2009, **1**, a002980.
3 C. W. Chang, Y. J. Cheng, M. Tu, Y. H. Chen, C. C. Peng, W. H. Liao and Y. C. Tung, *Lab Chip*, 2014, **14**, 3762.
4 C. Kim, K. Kreppenhofer, J. Kashef, D. Gradl, D. Herrmann, M. Schneider, R. Ahrens, A. Guber and D. Wedlich, *Lab Chip*, 2012, **12**, 5186-5194.
5 B. Y. Xu, S. W. Hu, G. S. Qian, J. J. Xu and H. Y. Chen, *Lab Chip*, 2013, **13**, 3714.
6 J. T. S. Fernandes, S. Tenreiro, A. Gameiro, V. chu, T. F. Outeiro and J. P. Conde, *Lab Chip*, 2014, DOI: 10.1039/c4lc00756e
7 S. Ostrovidov, N. Annabi, A. Seidi, M. Ramalingam, F. Dehghani, H. Kaji and A. Khademhosseini, *Anal. Chen.*, 2012, **84**, 1302-1309.
8 D. Kim and C. L. Haynes, *Anal. Chen.*, 2012, **84**, 6070-6078.
9 Y. H. Jang, M. J. Hancock, S. B. Kim. S. Selimovic, W. Y. Sim, H. Bae and A. Khademhosseini, *Lab Chip*, 2011, **11**, 3277.
10 W. Siyan, Y. Feng, Z. Lichuan, W. Jiarui, W. Yingyan, J. Li, L. Bingcheng and W. Qi, *J. Pharm. Biomed. Anal.*, 2009, **49**, 806-810.
11 C. J. Wang, X. Li, B. Lin, S. Shim, G. Ming and A. levchenko, *Lab Chip*, 2008, **8**, 227-237.
12 D. L. Englert, M. D. Manson and A. Jayaraman, *Appl. Environ. Microbiol.*, 2009, **75**, 4557.
13 D. L. Englert, M. D. Manson and A. Jayaraman, *Nature Protocol*, 2010, **5**, 864.
14 B. G. Ricart, B. John, D. Lee, C. A. Hunter and D. A. Hammet, *J Immunol.*, 2011, **186**, 53-61.
15 B. G. Chung, L. A. Flanagan, S. W. Rhee, P. H. Schwartz, A. P. Lee, E. S. Monuki and N. L. Jeon, *Lab Chip*, 2005, **5**, 401–406.
16 G. Zheng, Y. Wang and J. Qin, *Anal. Bioanal. Chem.*, 2012, **404**, 3061–3069.
17 J. Ruan, L. Wang, M. Xu, D. Cui, X. Zhuo and D. Liu, *Mater. Sci. Eng., C*, 2009, **29**, 674–679.
18 Aman Russom, D. Irimia and M. Toner, *Electrophoresis*, 2009, **30**, 2536-2543.
19 J. J. Vandersarl, A. M. Xu and N. A. Melosh, *Lab Chip*, 2011, **11**, 3057.
20 P. J. Hung, P. J. Lee, P. Sabounchi, R. Lin and L. P. Lee, *Biotechnol. Bioeng.*, 2005, **89**.
21 M. E. Brett, R. DeFlorio, D. E. Stone and D. T. Eddington, *Lab Chip*, 2012, **12**, 3127-3134.
22 T. Frank and S. Tay, *Lab Chip*, 2013, **13**, 1273.
23 H. Wu, B. Huang and R. N. Zare, *J. AM. CHEM. SOC.*, 2006, **128**, 4194-4195.
24 F. Piraino, G. C. Unal, M. J. Hancock, M. Rasponi and A. Khademhosseini, *Lab Chip*, 2012, **12**, 659.
25 J. He, Y. Du, J. L. Villa-Uribe, C. Hwang, D. Li and A. Khademhosseini, *Adv. Funct. Mater.*, 2010, **20**, 131-137.
26 Y. Du, J. Shim, M. Vidula, M. J. Hancock, E. Lo, B. G. Chung, J. T. Borenstein, M. Khabiry, D. M. Cropek and A. Khademhosseini, *Lab Chip*, **9**, 761-767.
27 M. Kim and T. Kim, *Anal. Chem.*, 2010, **82**, 9401–9409.
28 J. Atencia, G. A. Cooksey and L. E. Locascio, *Lab Chip*, 2012, **12**, 309.
29 J. Atencia, J. Morrow and L. E. Locascio, *Lab Chip*, 2009, **9**, 2707-2714.

30 U. Haessler, M. Pisano, M. Wu and M. A. Swartz, *PNAS*, 2011, **108**, 5614-5619.
31 U. Haessler, Y. Kalinin, M. A. Swartz and M. Wu, *Biomed Microdevices*, 2009, **11**, 827–835.
32 S. Y. Cheng, S. Heilman, M. Wasserman, S. Archer, M. L. Shuler and M. Wu, *Lab Chip*, 2007, **7**, 763–769.
33 E. Cimetta, C. Cannizzaro, R. James, T. Biechele, R. T. Moon, N. Elvassore and G. Vunjak-Novakovic, *Lab Chip*, 2010, **10**, 3277–3283.
34 T. Ahmed, T. S. Shimizu and R. Stocker, *Nano. Lett.*, 2010, **10**, 3379–3385.

